SIMULATIONS OF SNS ACCUMULATOR RING BEAM POSITION MONITOR SIGNALS

BNL/SNS TECHNICAL NOTE

NO. 038

J. Beebe-Wang, A. U. Luccio, R. Witkover

November 7, 1997

ALTERNATING GRADIENT SYNCHROTRON DEPARTMENT
BROOKHAVEN NATIONAL LABORATORY
UPTON, NEW YORK 11973

Simulations of SNS Accumulator Ring Beam position Monitor Signals

J. Beebe-Wang, A. U. Luccio and R. Witkover

AGS Department, Brookhaven National Laboratory, Upton, NY 11973, USA

1. Introduction

The most common method of monitoring beam position is to couple the electromagnetic field of the beam current with pickup electrodes. A conventional stripline beam position pickup is a pair of electrodes (or two pairs, if both transverse beam position coordinates are being measured) which cannot sense dc electromagnetic fields. The signals in the pickup electrodes are induced by beam current modulation. The carrier for the beam position information is the frequency (and harmonics) of the periodic beam bunches for a continuous train of bunches or the derivation of the instantaneous beam current for single bunches.[1]

In the current design of the Spallation Neutron Source (SNS), the particles are injected one pulse per turn into the accumulator ring during 1225 turns. The beam will have only one long bunch of 546 nsec with a rather flat longitudinal distribution. The Beam Position Monitors (BPM), associated with each quadrupole, will be implemented with conventional stripline electrodes. To determine whether the currently designed BPM can serve the purpose of monitoring such beam, two questions need to be answered: (1) would the signal be strong enough at the beginning of the injection when the beam current is small; (2) would the derivation of the signal be big enough when a long flat longitudinal bunch shape is developed in the later stage of the injection. A simulation study of the signals in the BPM of the SNS accumulator ring was performed in an attempt to answer these two questions. This note reports the results of the simulation and the signal analysis.

2. Electrode Signals in a Stripline

Stripline electrodes are essentially transmission lines with well-defined characteristic impedance and with a segment of the center conductor exposed to the beam. Consider an electrode of azimuthal width ϕ, length l, and characteristic impedance Z in a cylindrical beam pipe of radius b as shown in Fig. 1. We examine the signal formation on this stripline electrode in both time and frequency domains.

2.1 Signals from a centered beam

If the beam current is $I_b(t)$, the wall current intercepted by the stripline electrode with azimuthal widthϕ is $(\phi / 2\pi) I_b(t)$. When the beam pulse approaches the upstream end of the

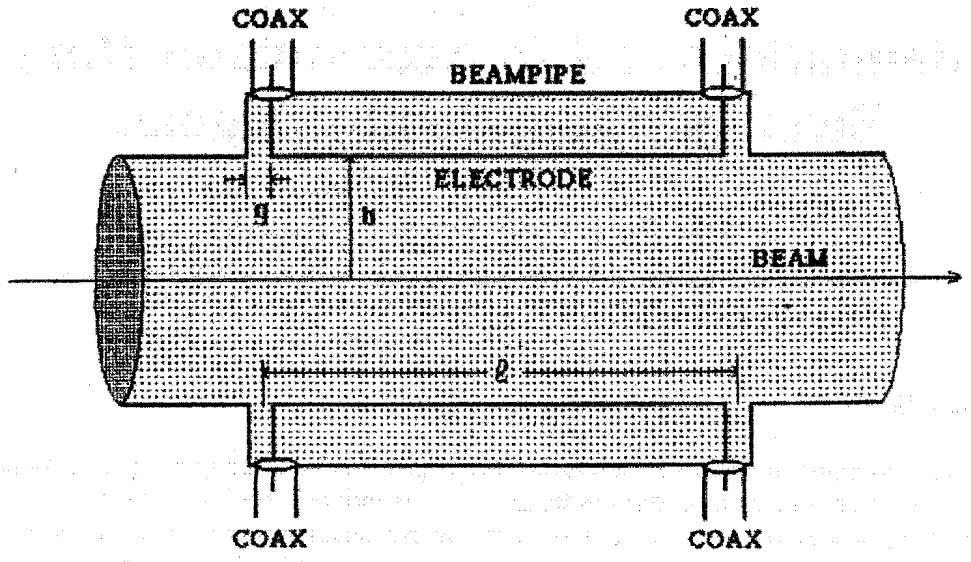

Figure 1. Side view of a stripline beam position electrode. The electrode is a section of an impedance-matched transmission line with the center conductor exposed to the image fields of the passing beam.

electrode, the voltage $V(t) = (\phi / 2\pi) I_b(t) Z / 2$ induced across the gap launches TEM waves in two directions. One signal goes out from the upstream port to the electronics. The other wave travels down the outside surface of the electrode to the downstream port at a signal velocity $v_s = \beta_s c$ and out from the downstream port. The beam travels down the beam pipe at velocity $v_b = \beta_b c$ and induces a similar signal at the downstream gap, with a delay $l / \beta_b c$ and an opposite polarity to the first one. The net result at the upstream port is:

$$V_U(t) = \frac{\phi Z}{4\pi}\left[I_b(t) - I_b(t - \frac{l}{\beta_b c} - \frac{l}{\beta_s c}) \right] \tag{1}$$

and at the downstream port:

$$V_D(t) = \frac{\phi Z}{4\pi}\left[I_b(t - \frac{l}{\beta_s c}) - I_b(t - \frac{l}{\beta_b c}) \right] \tag{2}$$

2.2 Signals from off-centered beams

We first investigate what happens to the wall currents when the beam is displaced from the center of a circular beam pipe. Laplace equation can be solved in two dimensions to find the wall current density for a pencil beam current $I_b(t)$ at position (r,θ) inside a grounded circular conducting beam pipe of radius b.[2] The wall current density i_w at time t and location (b,ϕ_w) is then:

$$i_w(b,\phi_w,t)=\frac{-I_b(t)}{2\pi b}\left\{1+2\sum_{n=1}^{\infty}\left(\frac{r}{b}\right)^n\cos\left[n(\phi_w-\theta)\right]\right\} \tag{3}$$

If two electrodes (L and R for left and right) of angular width ϕ are placed at 0° and 180° as shown in Fig. 2, the resultant currents flowing parallel to the beam on the inside surface of these electrodes are:

$$i_R(t)=\frac{-I_b(t)\phi}{2\pi}\left\{1+\frac{4}{\phi}\sum_{n=1}^{\infty}\frac{1}{n}\left(\frac{r}{b}\right)^n\cos(n\theta)\sin\left(\frac{n\phi}{2}\right)\right\} \tag{4}$$

and

$$i_L(t)=\frac{-I_b(t)\phi}{2\pi}\left\{1+\frac{4}{\phi}\sum_{n=1}^{\infty}\frac{1}{n}\left(\frac{r}{b}\right)^n\cos(n\theta)\sin\left(n(\pi+\frac{\phi}{2})\right)\right\} \tag{5}$$

The electrode response to a beam displacement x (for $\theta=0$) is:

$$\frac{i_R-i_L}{i_R+i_L}=\frac{4\sin(\phi/2)}{\phi}\frac{x}{b}+\text{Higher order terms.} \tag{6}$$

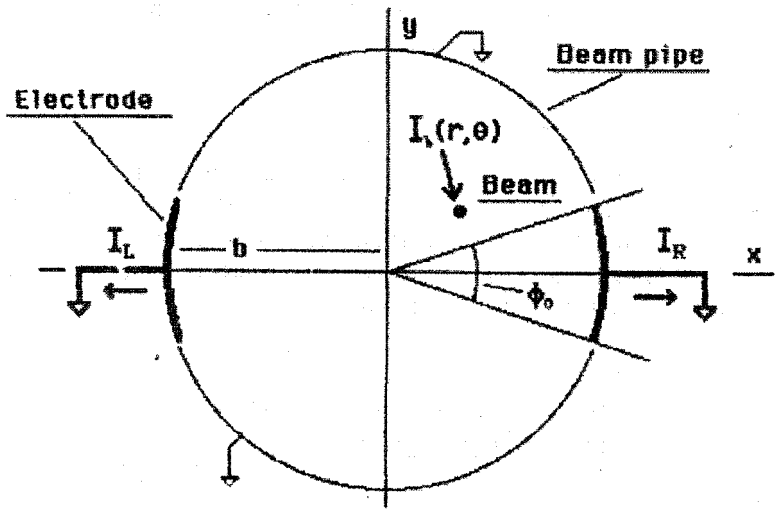

Figure 2. Cross section of stripline electrode model used for the simulation.

3. Computer Simulation of the SNS Accumulator Ring BPM signals

The computer simulation study was performed with the computer code ACCSIM, developed at TRIUMF[3]. The code tracks a large number of macro particles through the lattice, in the presence of space charge forces and beam to wall interactions, in full 6-dimensions. The lattice is the current 4-fold accumulator ring design[4] and all the physical quantities used in the simulation are chosen to be as close as possible to the specifications in the current Conceptual Design Report. The lattice functions and other salient design parameters of the BPM and the accumulator ring used in the simulation are summarized in Table I. The number of macro particles is generally set to 10^5~10^6 which is limited by computer run time.

Table 1. The SNS accumulator ring injection and BPM design parameters used in this simulation study.

SNS Accumulator Ring Injection		BPM Stripline Electrode	
Number of turns injected	1225	Electrode length l	20 cm
Beam gap (injection)	295 nsec	Electrode azimuthal width ϕ	70^0
Injected pulse length	546 nsec	Characteristic impedance Z	50 Ω
Rise/fall time of the pulse	2 nsec	Beam pipe radius b	10 cm

The SNS accumulator ring receives injected pulses with length of 546 nsec, rise/fall time of 2 nsec, and inter bunch gap of 295 nsec. The beam position monitors use dual plane stripline electrodes with open circuit at the downstream end to allow their use as clearing electrodes. Each electrode has a length l=20 cm, an azimuthal width ϕ=70^0 and a characteristic impedance Z=50 Ω. The average beam pipe radius b=10 cm is assumed in this simulation study.

The most important factors that determine the form of the BPM signals are the longitudinal particle distribution at injection and the RF waveform.

3.1 Density distribution at injection

Distributions of injected particles are separately generated in the horizontal, vertical and longitudinal coordinate systems. Two methods are used in ACCSIM to generate distributions: a simple "masked rectangle" method for uniform distributions and a general binomial distribution method[5] for a range of distribution profiles. We used the second method in the simulation in order to generate the distribution as close as possible to the injected pulses in the SNS accumulator ring.

If we specify ε as the emittance of the ellipse that contains 2 standard deviations (in each dimension) of the beam, the bounding rectangle is given by

$$\Delta X = \sqrt{\frac{m+1}{2}}\sqrt{\varepsilon\beta}$$
$$\Delta X' = \sqrt{\frac{m+1}{2}}\sqrt{\varepsilon\gamma} \qquad (7)$$

where m is the binomial distribution parameter. A point in the ellipse was generated from two given random numbers R_1 and R_2 in the range [0,1] in the following way:

$$\Delta x = a\cos b\Delta X \tag{8}$$

$$\Delta x' = (a\cos b\sin\chi + a\sin b\cos\chi)\Delta X' \tag{9}$$

where $a = \sqrt{1-R_1^{1/m}}$, $b = 2\pi R_2$ and χ is the ellipse tilt parameter given by

$$\cos\chi = \sqrt{\frac{1}{1+\alpha^2}} \tag{10}$$

and

$$\sin\chi = -\alpha\cos\chi\,. \tag{11}$$

This method was used in the same way to generate distributions in the horizontal, vertical and longitudinal planes. However, in the longitudinal plane the beam ellipse is assumed to have no tilt and is always specified by half widths. For each particle, the procedures generate a set of displacements $(\Delta x, \Delta x', \Delta y, \Delta y', \Delta\phi, \Delta(\Delta E))$ from the current location of the injected beam center $(x_0, x'_0, y_0, y'_0, \phi_0, \Delta E_0)$. These displacements are then added to the center coordinates to obtain the actual injection coordinates $(x, x', y, y', \phi, \Delta E)$ for the particle.

Table 2. Properties of binomial phase space distribution.

m	Distribution	Phase Space Density $\rho(u,v)$, $a^2 \equiv u^2 + v^2$	Profile $f(u) = \int_{-\infty}^{+\infty} \rho(u,v)dv$	% of beam outside of 2σ ellipse
0.0	K-V	$\frac{1}{\pi}\delta(1-a^2)$	$\frac{1}{\pi}(1-u^2)^{-0.5}$	0
0.5	Flat	$\frac{1}{2\pi}(1-a^2)^{-0.5}$	$\frac{1}{2}$	0
1.0	Uniform	$\frac{1}{\pi}$	$\frac{2}{\pi}(1-u^2)^{0.5}$	0
1.5	Elliptical	$\frac{3}{2\pi}(1-a^2)^{0.5}$	$\frac{3}{4}(1-u^2)$	8.9%
2.0	Parabolic	$\frac{2}{\pi}(1-a^2)$	$\frac{8}{3\pi}(1-u^2)^{1.5}$	11.1%
$\to\infty$	Gaussian	$\frac{1}{2\pi\sigma\sigma'}\exp\left(-\frac{x^2}{2\sigma^2}-\frac{x^2}{2\sigma'^2}\right)$	$\frac{1}{\sqrt{2\pi}\sigma}\exp\left(-\frac{x^2}{2\sigma^2}\right)$	12.8%

The shape of the binomial distribution is governed by a single parameter m. Varying m yields various common distribution types, approaching a Gaussian as $m \to \infty$. For a finite m, the distribution has a finite range and is therefore preferable to a Gaussian for simulation purposes. To make it easier to understand the kinds of distributions associated with m values, for some common values of m, we list the distribution shape, the profile shapes (1-D projected distribution) and the amount of beam that lies outside the 2σ ellipse in Table 2. We need to choose a suitable m value, so that the presentation of the particle distribution in the injected pulse is as close as possible to the reality.

The injection is done with a chopper of rise/fall time of 2 nsec with pulse length of 546 nsec and beam gap 295 nsec. The linac beam has a 402.5 MHz microstructure, which means that there are 220 micro pulses in one injected pulse of 546 nsec. The particle density distribution is governed by the profile shapes other than the distribution shapes due to this microstructure. In the present simulation, the microstructure was considered to determine the bunch shape at the injection, but not considered at the later stages. In Fig. 3, we illustrate 3 different profile shapes corresponding to m=0.5, 1.02 and 3.0 respectively. We chose m=1.0352 in the simulation to give a rise/fall time of 2 nsec. Here we define rise/fall time to be the time it takes for a pulse to rise/fall to 85% of its maximum current (the current at the center of the bunch).

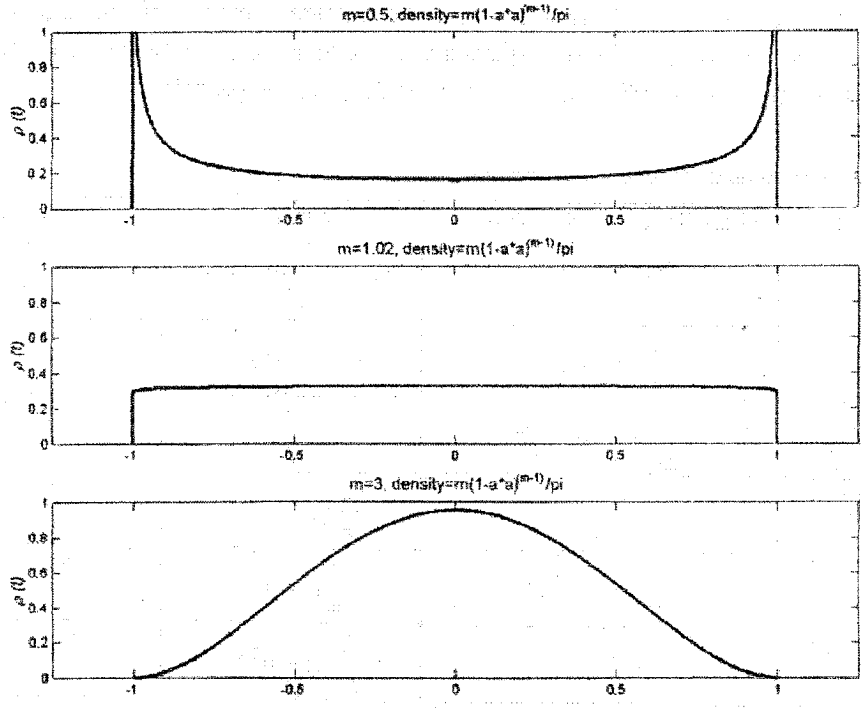

Figure 3. The logitudinal profile shapes of a long bunch corresponding to m=0.5, 1.02 and 3.0 respectively.

3.2 The RF systems

Previous work[6,7] has established that a dual-frequency RF system with harmonics $h=1$ and $h=2$ has significant advantages over a single-frequency system. A barrier bucket RF system is even better, but there are unresolved issues, such as beam loading, that will require more R&D. Therefore, the base design for the SNS RF system is a dual harmonic system running with $h=1$ and $h=2$. Following the current design, the RF system used in this simulation study has amplitudes of 40 kV at $h=1$ and 20 kV at $h=2$, with 180^0 phase advance. In order to investigate the different effects caused by dual-frequency RF and single-frequency RF system, a simulation with single-frequency of 60 kV at $h=1$ was also performed with other conditions identical as the dual-frequency RF cases. Both RF waveforms are shown in Fig. 4.

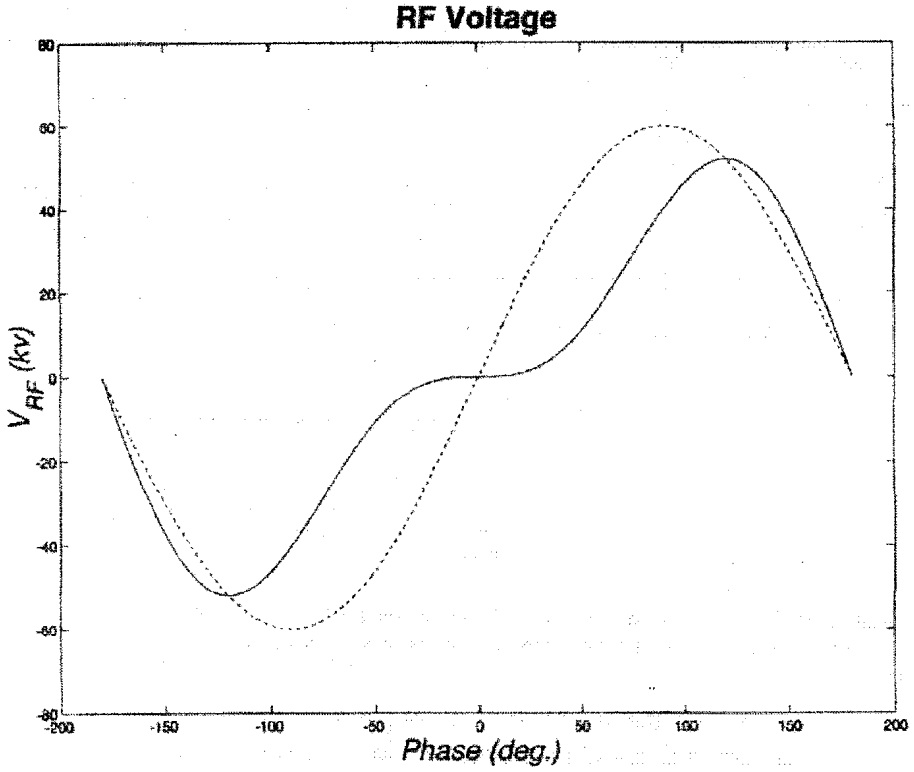

Figure 4. RF waveforms of SNS accumulator ring. The solid line represents s the dual -frequency case. The dotted line is for the signal-frequency case.

4. BPM Signal Analysis

From the longitudinal particle distribution obtained from ACCSIM tracking, BPM signals are constructed by using eq.(1). Fig. 5 shows the signals at the upstream port of stripline electrodes after 1, 100, 500 and 1225 turns during the injection, where the solid lines represent the dual-frequency RF case and the dotted lines are for the single-frequency RF case. It is easy

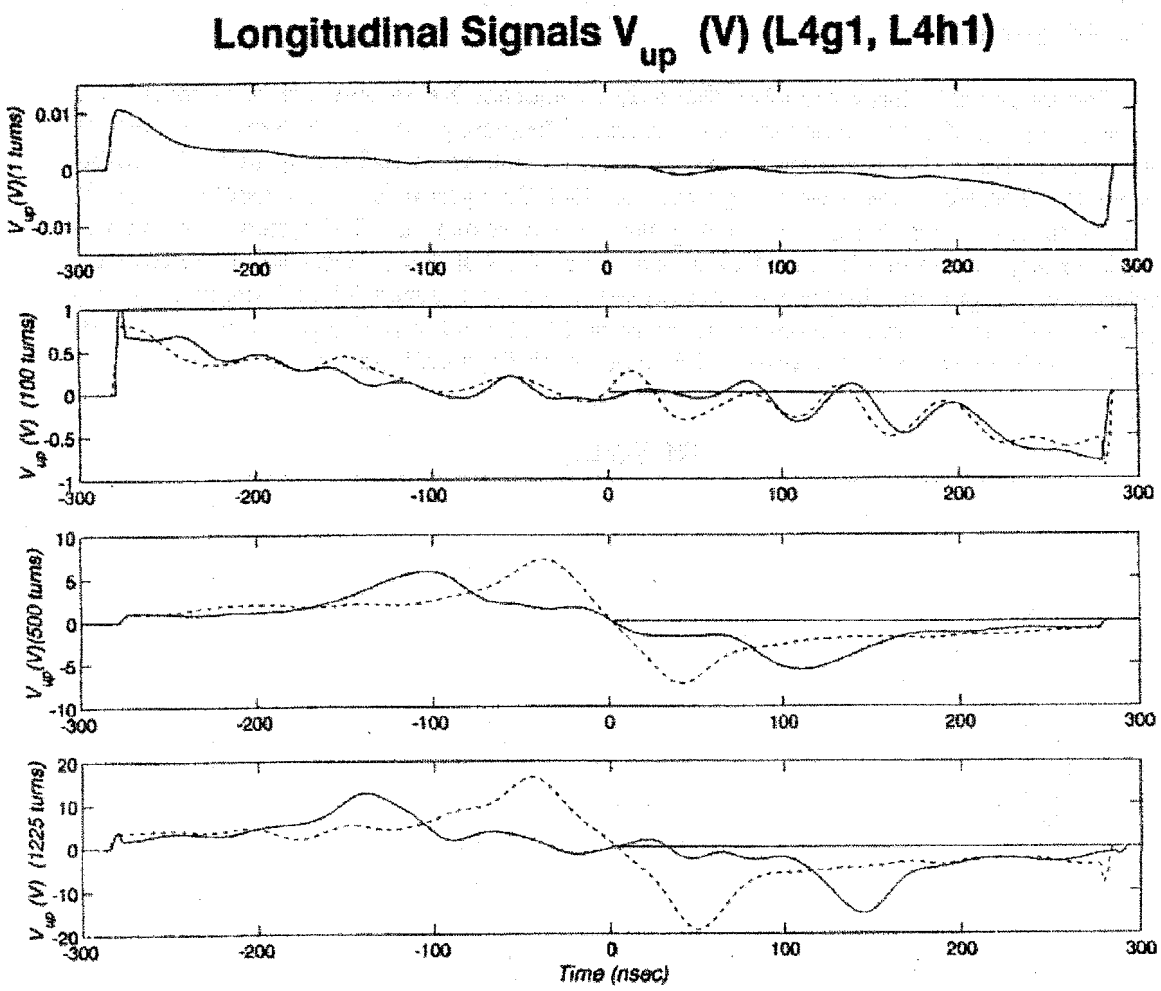

Figure 5. BPM signals at the upstream port of stripline electrodes after 1, 100, 500 and 1225 turns during the injection. The solid lines represent the dual-frequency RF case and the dotted lines are for the single-frequency RF case.

to see that, at the beginning of the injection, the longitudinal distribution of the bunch is governed by the injection distribution and the signals are indistinguishable for the two cases and, at a later stage, the single-frequency RF produces a more centrally concentrated bunch shape, while the dual-frequency RF produces a more evenly distributed beam.

The FFT spectrums of the signals at the corresponding stages are shown in Fig. 6. The most important observation is that the higher order harmonics do not vanish fast due to the complicated shape of the signals. Fig. 7 and Fig. 8 show the relative amplitude and relative phase of the first four harmonics, respectively. The major conclusion we can make from these figures is that the higher harmonics are large compared to the first harmonic and the relative phases change rapidly in a large range of $[-\pi, \pi]$ which may make the analysis of the signal very difficult.

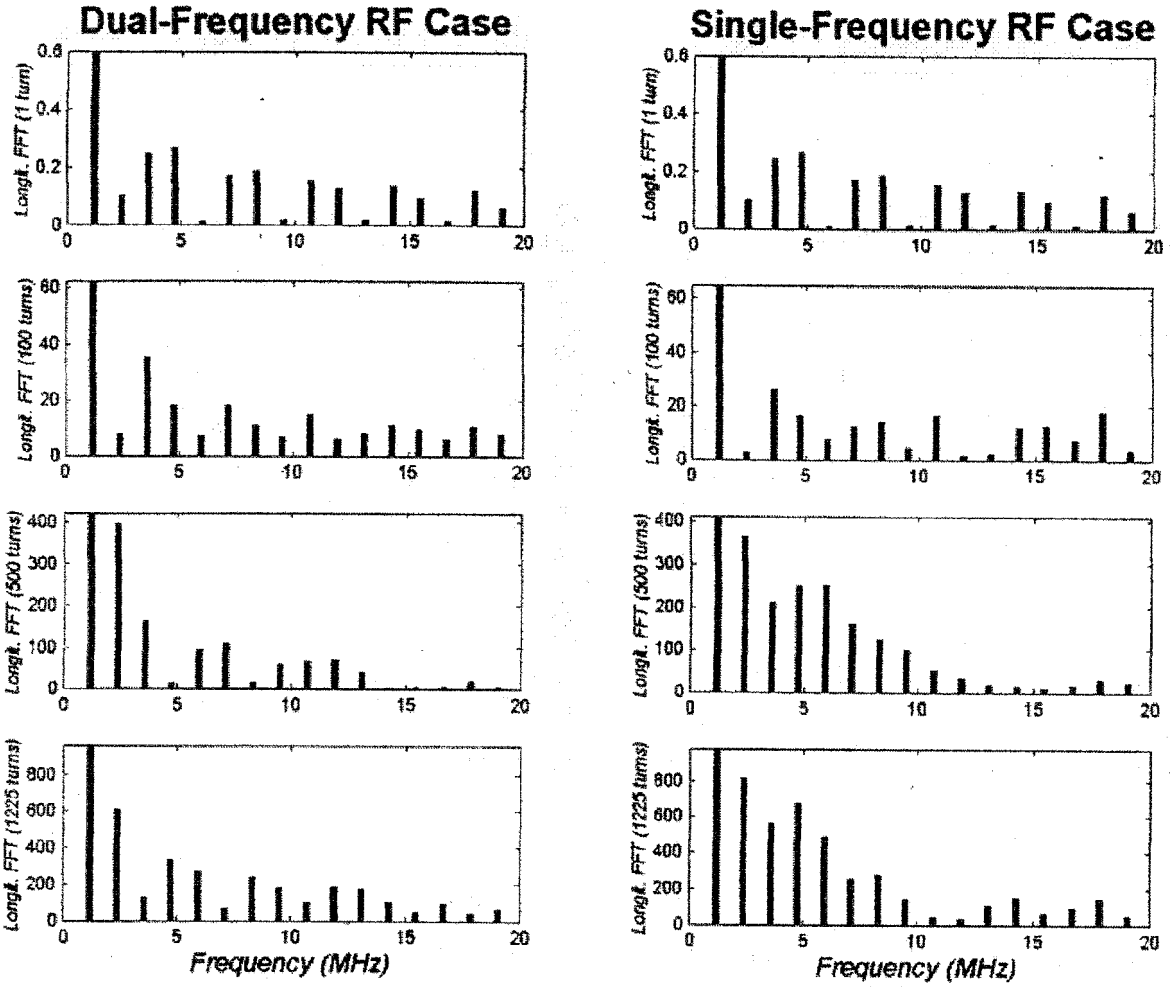

Figure 6. The FFT spectra of BPM signals (shown in Fig. 5) after 1, 100, 500 and 1225 turns during the injection. The dc components are zero. The maximum values on the vertical scales are set to be the same as the amplitude of the first harmonic.

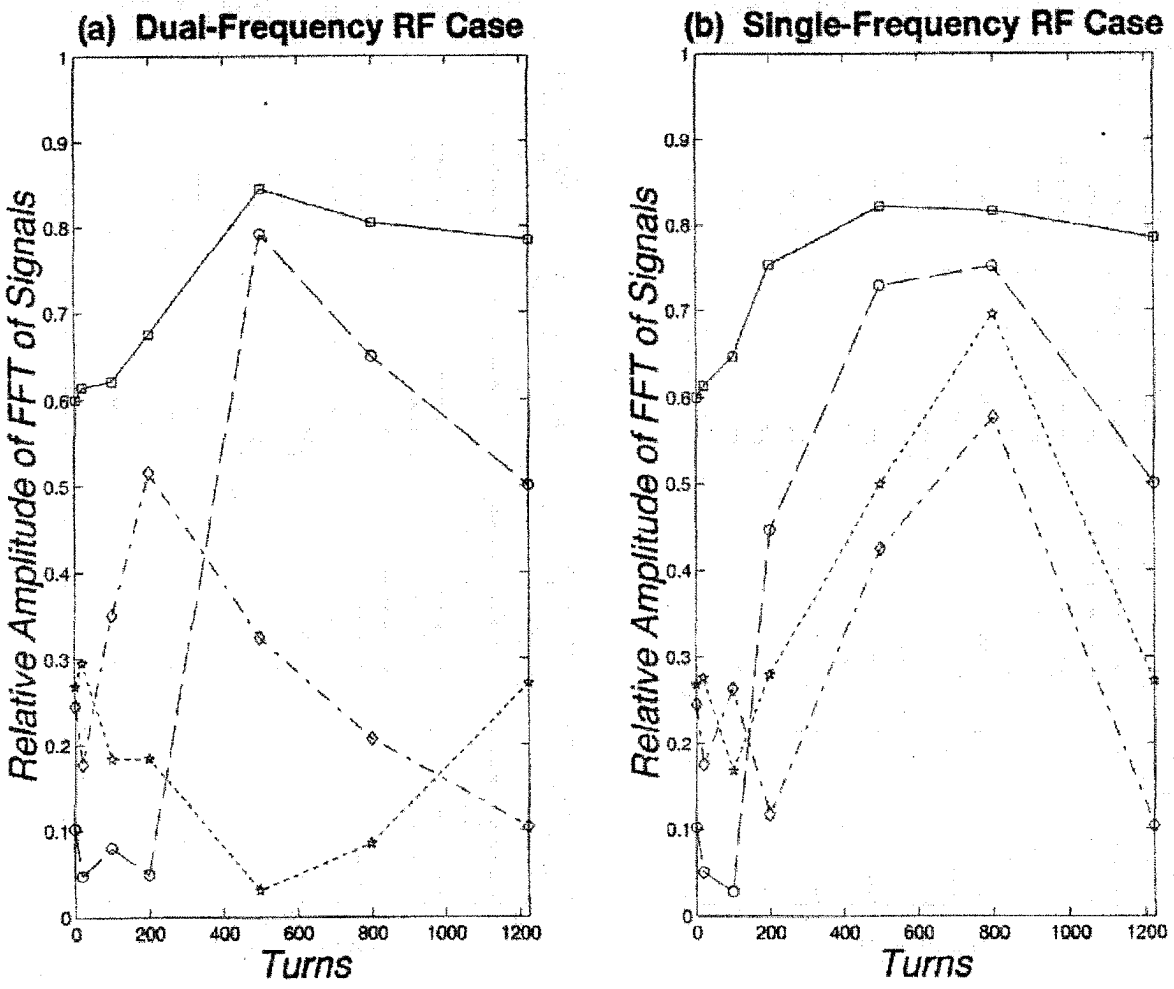

Figure 7. The relative amplitude of the first four harmonics of the FFT spectra of the BPM signal (as shown in Fig. 6). The square markers and the solid line represent the 1st harmonic; the circle markers and the dashed line represent the 2nd harmonic; the diamond markers and the dash-dot line represent the 3rd harmonic and the pentagram markers and the dotted line represent the 4th harmonic.

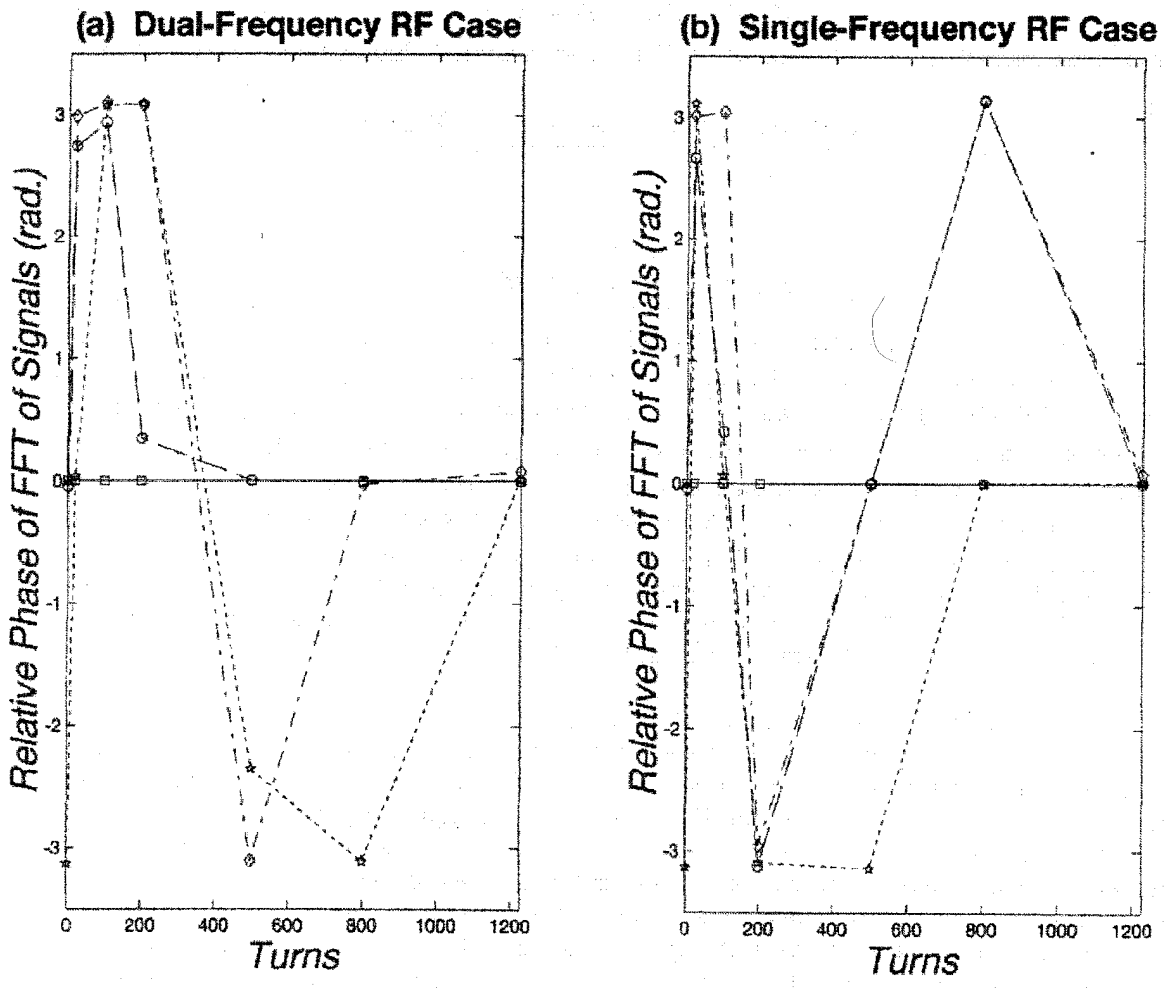

Figure 8. The relative phase of the first four harmonics of the FFT spectra of the BPM signal (as shown in Fig. 6). The square markers and the solid line represent the 1st harmonic; the circle markers and the dashed line represent the 2nd harmonic; the diamond markers and the dash-dot line represent the 3rd harmonic and the pentagram markers and the dotted line represent the 4th harmonic.

In order to find another alternative, we attempted to reconstruct the beam current $I_b(t)$ from the signal $V_U(t)$. Let $V(t') = \frac{\phi Z}{4\pi} I_b(t')$ and $t' = t - \Delta t$ where $\Delta t = \frac{l}{\beta_b c} + \frac{l}{\beta_s c}$, then eq. (1) can be rewritten as

$$V_U(t') = V(t'+\Delta t) - V(t') \quad . \tag{12}$$

If the time interval Δt is small over which $V(t')$ is approximately linear, we can express $V_U(t')$ by:

$$V_U(t') = \frac{V(t'+\Delta t) - V(t')}{\Delta t}\Delta t \approx \frac{dV(t')}{dt'}\Delta t = \frac{\phi Z}{4\pi}\frac{dI_b(t')}{dt'}\Delta t \quad , \tag{13}$$

or

$$I_b(t') = \frac{4\pi}{\phi Z \Delta t}\int V_U(t')dt' \quad , \tag{14}$$

which means that the beam current $I_b(t')$ can be reconstructed from $V_U(t')$ through an integral. The current design of the SNS accumulator ring BPM yields $\Delta t = 0.76$ nsec. It is easy to see from Fig. 5 that $V(t')$ is approximately linear over this time interval. So, with a proper on-line integrator circuit, we can reconstruct the beam current $I_b(t')$ by integrating the signals obtained from the upstream port. As an example, in Fig. 9, we show the reconstructed beam current $I_b(t')$ at 1, 100, 500 and 1225 turns during the injection from the signals shown in Fig. 5. By investigate Fig. 9, we can see that, in both dual-frequency RF and single-frequency RF cases, the longitudinal distribution of the bunch is governed by the injection distribution at the beginning stage of the injection. The bunches start to have distinguishable longitudinal shapes and start to develop tails around the 100th turn for both cases.

The FFT of the beam currents at the corresponding stages are shown in Fig. 10. Now, one can see that the higher order harmonics vanish much faster compared to Fig. 6. Relative amplitude and relative phase of the first four harmonics are plotted in Fig. 11 and Fig. 12 respectively. In order to compare the FFT result from the signals, the relative amplitudes are scaled to have the same first harmonic value. From Fig. 11 we can see that only the first and second harmonics are of importance and change in the same way during the injection. From Fig. 12 we also can see that the phase relationship between the harmonics are more stable. For example, the relative phase between the second and the first harmonic is in the range of [-0.4, 0.4] compared to $[-\pi, \pi]$ obtained from the signal. All of these make FFT analysis much easier.

It seems, from the results of this simulation study that the signals induced in the BPM electrode may be strong enough to serve the purpose of monitoring SNS accumulator ring beams, because at the beginning stage of the injection, when the beam current is small, the bunches have sharp longitudinal boundary which triggers strong signal in the electrode, and after the longitudinal tails are developed (after the 100th turn) the beam current is bigger which yields to higher signal/noise ratio. However, this study only shows the signals at the upstream port of the electrode before going into electronics. The final signals are also limited by the

specifications of electronics. We would also like to investigate what effect it could have on the BPM signals due to phase space painting during the injection.

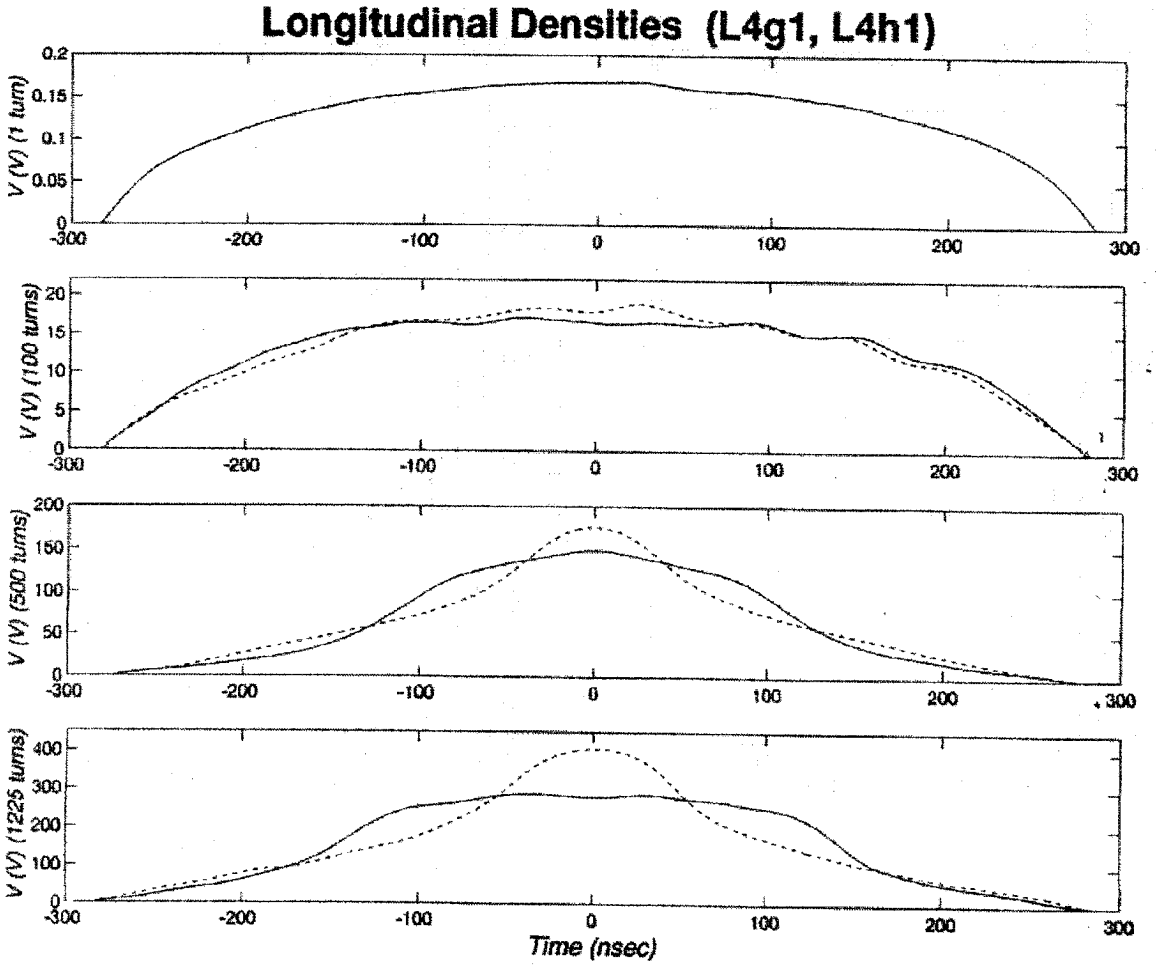

Figure 9. Integral of BPM signals at the upstream port of stripline electrodes after 1, 100, 500 and 1225 turns during the injection. The solid lines represent the dual-frequency RF case and the dotted lines are for the single-frequency RF case.

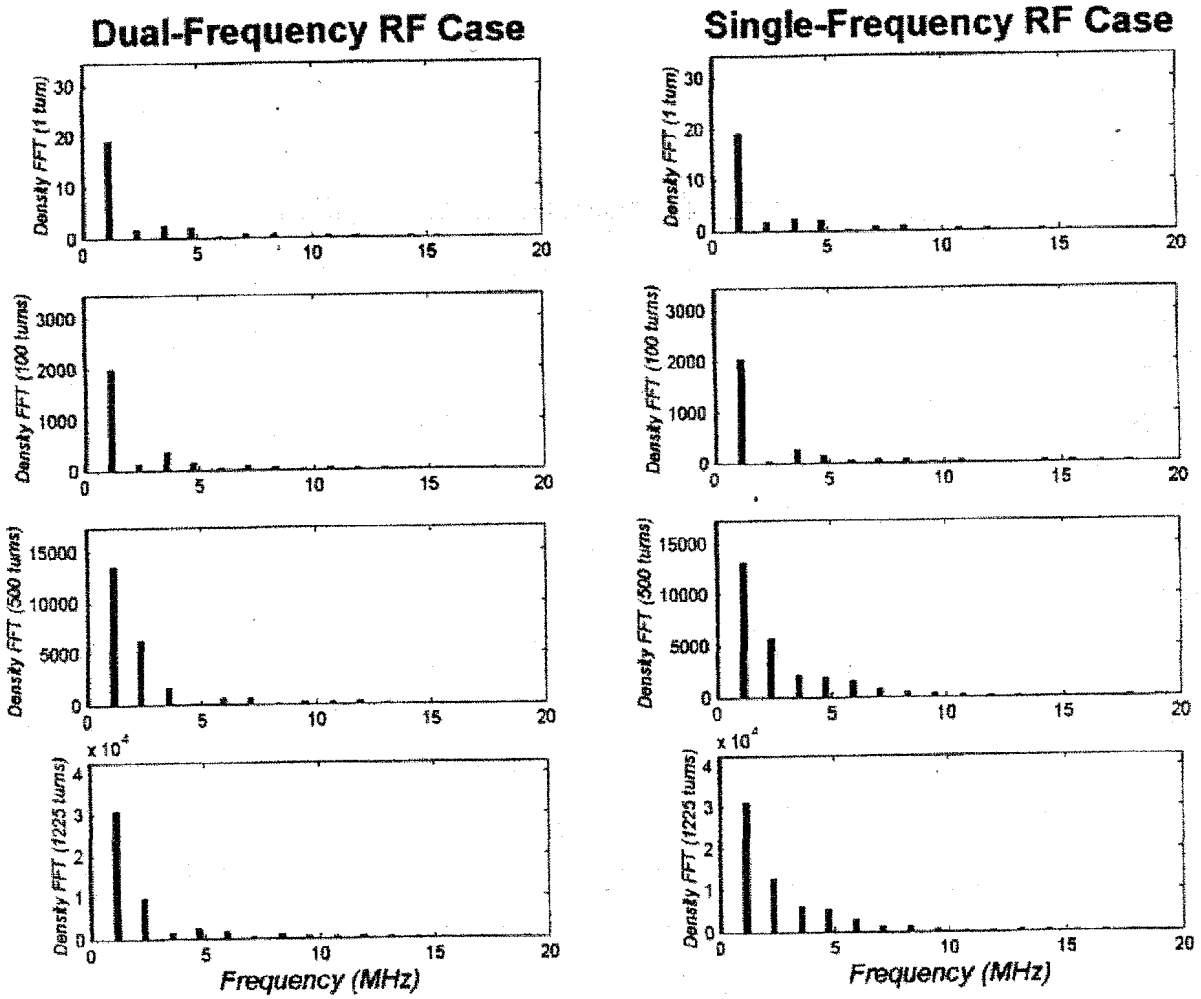

Figure 10. The FFT spectra of the integral of the BPM signals (shown in Fig. 9) after 1, 100, 500 and 1225 turns during the injection. The dc components are non-zero. The maximum values on the vertical scales are set to be the same as the amplitude of the dc components.

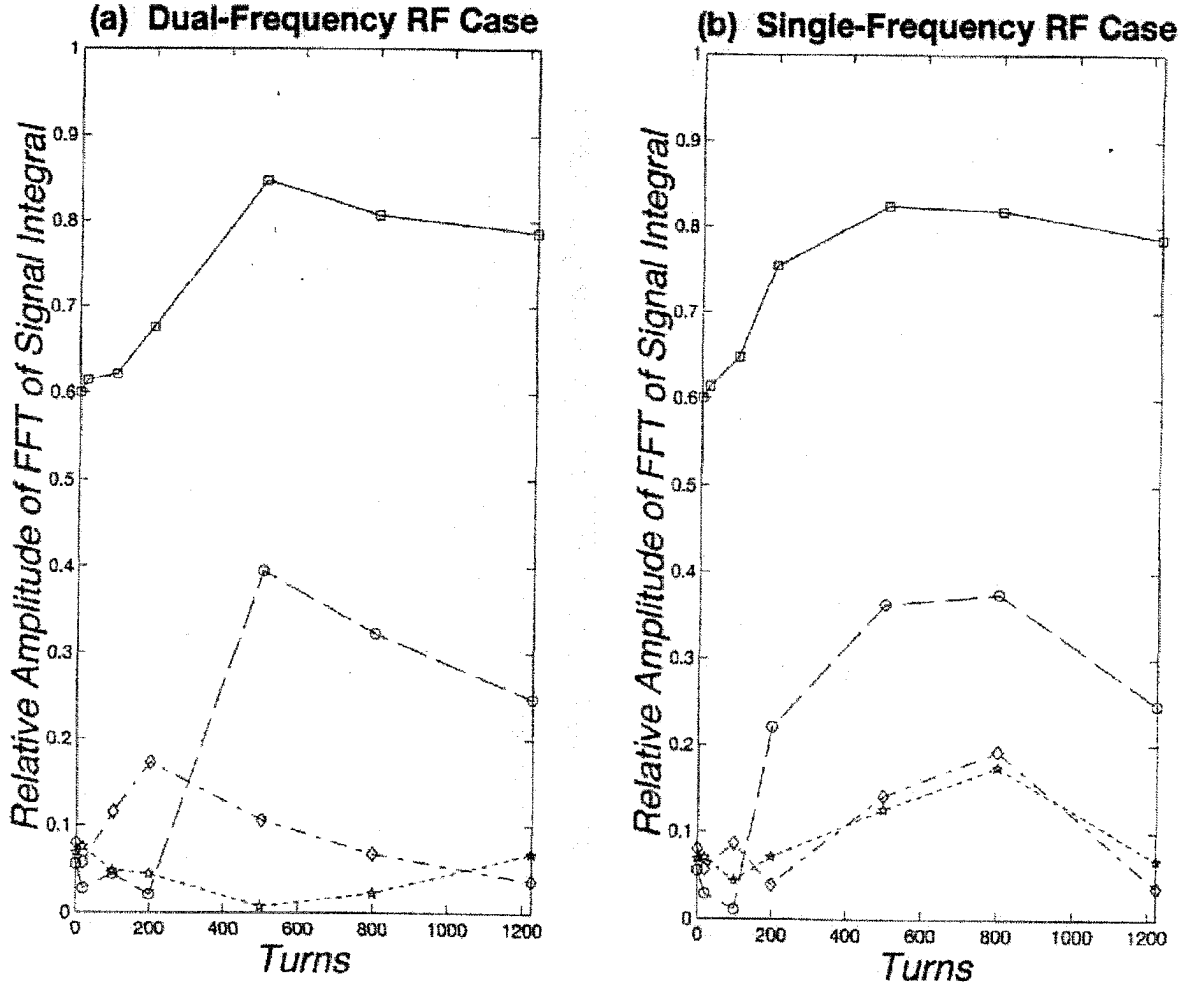

Figure 11. The relative amplitude of the first four harmonics of the FFT spectra of the BPM signal integral (shown in Fig. 10). The square markers and the solid line represent the 1st harmonic; the circle markers and the dashed line represent the 2nd harmonic; the diamond markers and the dash-dot line represent the 3rd harmonic and the pentagram markers and the dotted line represent the 4th harmonic.

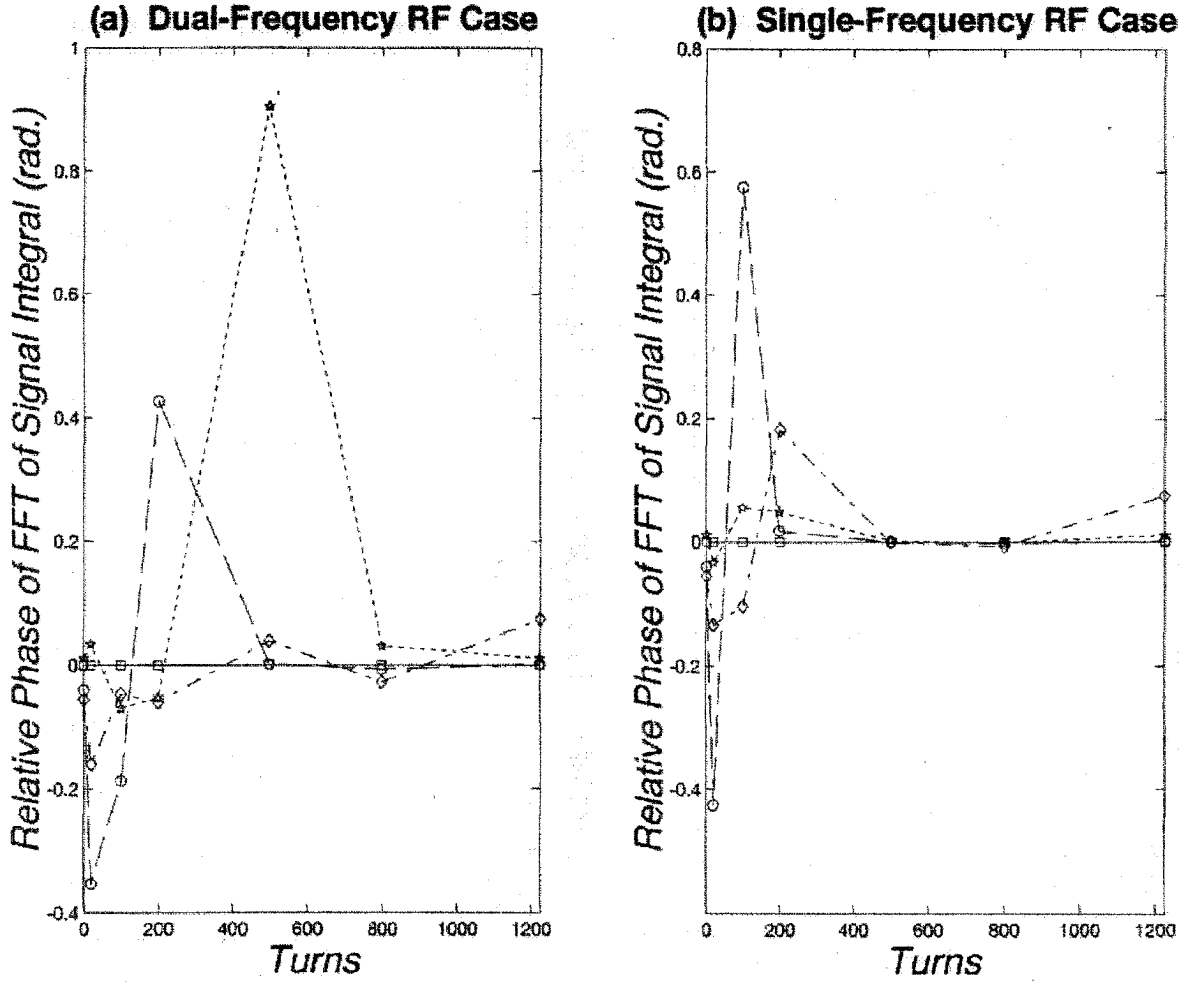

Figure 12. The relative phase of the first four harmonics of the FFT spectra of the BPM signal integral (shown in Fig. 10). The square markers and the solid line represent the 1st harmonic; the circle markers and the dashed line represent the 2nd harmonic; the diamond markers and the dash-dot line represent the 3rd harmonic and the pentagram markers and the dotted line represent the 4th harmonic.

5. References

1. R. E. Shafer, "Beam Position Monitoring", in "AIP Conference proceedings 212, Accelerator Instrumentation" edited by E. R. Beadle and V. J. Castillo, Upton, NY, 1989.

2. R. E. Shafer, "Characteristics of Directional Coupler Beam Position Monitors", IEEE Trans. Nucl. Sci. 32, p1933 (1985).

3. F. W. Jones, "User's Guide to ACCSIM", TRIUMF Design Note TRI-DN-90-17, June 1990 (and later additions).

4. W. T. Weng *et al*, "Accumulator Ring Design for the NSNS Project", in "Proceedings of 1997 Particle Accelerator Conference", Vancouver, B. C., Canada, 12-16 may, 1997.

5. W. Joho, "Representation of Beam Ellipses for Transport Calculations", SIN-REPORT TM-11-14, 8.5.1980.

6. M. Blaskiewicz, J. M. Brennan and Y. Y. Lee, "RF Options for the NSNS", BNL/NSNS Technical Note No. 009, December 5, 1996.

7. M. Blaskiewicz, J. M. Brennan and A. Zaltsman, "The NSNS RF System", BNL/NSNS Technical Note No. 036, May 12, 1997.